A Population Study of Common Ocular Abnormalities in C57BL/6N *rd8* Mice

Bret A. Moore,[1] Michel J. Roux,[2–5] Lionel Sebbag,[1] Ann Cooper,[1] Sydney G. Edwards,[1] Brian C. Leonard,[1] Denise M. Imai,[6] Stephen Griffey,[6] Lynette Bower,[7] Dave Clary,[7] K. C. Kent Lloyd,[7,8] Yann Hérault,[2–5,9] Sara M. Thomasy,[10,11] Christopher J. Murphy,[10,11] and Ala Moshiri[11]

[1]William R. Pritchard Veterinary Medical Teaching Hospital, School of Veterinary Medicine, University of California-Davis, Davis, California, United States
[2]Institut de Génétique et de Biologie Moléculaire et Cellulaire, Université de Strasbourg, Illkirch, France
[3]Centre National de la Recherche Scientifique, UMR7104, Illkirch, France
[4]Institut National de la Santé et de la Recherche Médicale, U964, Illkirch, France
[5]Université de Strasbourg, Illkirch, France
[6]Comparative Pathology Laboratory, School of Veterinary Medicine, UC Davis, Davis, California, United States
[7]Mouse Biology Program, University of California-Davis, Davis, California, United States
[8]Department of Surgery, School of Medicine, University of California-Davis, Sacramento, California, United States
[9]CELPHEDIA, PHENOMIN, Institut Clinique de la Souris (ICS), CNRS, INSERM, Université de Strasbourg, Illkirch, France
[10]Department of Veterinary Surgical and Radiological Sciences, School of Veterinary Medicine, UC Davis, Davis, California, United States
[11]Department of Ophthalmology & Vision Science, School of Medicine, University of California-Davis, Sacramento, California, United States

Correspondence: Ala Moshiri, Department of Ophthalmology and Vision Science, School of Medicine, University of California-Davis Eye Center, 4860 Y. Street, Suite 2400, Sacramento, CA 95817, USA; amoshiri@ucdavis.edu.
Christopher J. Murphy, Department of Surgical and Radiological Sciences, School of Veterinary Medicine, Department of Ophthalmology & Vision Science, School of Medicine, University of California at Davis, 1 Shields Avenue, Tupper Hall, Davis, CA 95616, USA; cjmurphy@ucdavis.edu.

Submitted: November 29, 2017
Accepted: March 11, 2018

Citation: Moore BA, Roux MJ, Sebbag L, et al. A population study of common ocular abnormalities in C57BL/6N *rd8* mice. *Invest Ophthalmol Vis Sci*. 2018;59:2252–2261. https://doi.org/10.1167/iovs.17-23513

Purpose. The purpose of this study was to quantify the frequency and severity of ocular abnormalities affecting wild-type C57BL/6N mice, the most common strain used worldwide for the creation of single-gene knockouts.

Methods. A total of 2773 animals (5546 eyes) were examined at one colony at UC Davis and in three more colonies at the Institut Clinique de la Souris in Strasbourg, France. Mice were examined at 15 to 16 weeks postnatal age by performing anterior segment biomicroscopy, posterior segment examination by indirect ophthalmoscopy, intraocular pressure measurement, and optical coherence tomography of anterior and posterior segment structures.

Results. Common ocular findings in the C57BL/6N strain included corneal deposits (3%), increased optical density of the anterior lens capsule (67%), punctate nuclear cataracts (98%), vitreous crystalline deposits (61%), hyaloid vascular remnant (6%), and retinal dysplasia attributed to the *rd8* mutation (58%). Interestingly, retinal dysplasia was more common in male mice in all four breeding colonies evaluated in this study. The thickness of ocular tissues and compartments were measured by spectral-domain optical coherence tomography, including the central cornea, anterior chamber, vitreous, and retinal layers. Intraocular pressure was measured by rebound tonometry.

Conclusions. Ocular abnormalities are common in anterior and posterior segments of the C57BL/6N mouse, the most common background on which single-gene knockout mice have been made. It is important that vision scientists understand the extent and variability of ocular findings associated with this particular genetic background of mice.

Keywords: knockout animals, mouse models, genetic diseases, morphometry, optical coherence tomography

The International Mouse Phenotyping Consortium (IMPC) was established in 2011 as a cooperative association of highly specialized academic centers with expertise in high-throughput mouse mutagenesis and/or comprehensive phenotyping.[1] The goal of the IMPC is to create the first functional encyclopedia of the mammalian genome modeled by the laboratory mouse.[2] At this time there are 15 participating laboratories in 12 countries around the globe. As of January 2017, the IMPC has produced fully validated single-deletion knockout mouse lines for 6000 genes, and has completed first-tier phenotyping across 11 body systems for 5000 of these genes.

Throughout the IMPC, the C57BL/6N strain of mice is used for the systematic production of all mouse knockouts. As a result of the IMPC being committed to the C57BL/6N strain of mice for their systematic production of knockouts, this strain is currently the most common background on which knockout mice are being produced and studied worldwide. However, genetic backgrounds influence the type and variability of strain-associated lesions, making it critical for researchers to be familiar with common background abnormalities seen in a

given strain. In particular, several background lesions in the eyes of the C57BL/6N mouse strain have been identified.[3] These background ocular findings include anterior corneal stromal deposits, incipient nuclear cataracts, altered translucency of the anterior lens capsule, vitreous crystalline deposits, and vitreous pigment. Therefore, phenotypic screening of all mice requires an intimate knowledge of C57BL/6N background ocular lesions to distinguish them appropriately. Additionally, C57BL/6N mice are homozygous for the *rd8* mutation in *Crb1*,[4] Crumbs homolog 1 gene, a mouse ortholog of the Drosophila Crumbs gene.[5] This mutation leads to a characteristic but variably severe retinal dysplasia that is most prominent in the inferior retina. The lesions appear as white to yellow flecks on fundus examination, and the phenotype is worsened by light exposure.[6]

The *rd8* mutation is widely known to exist in C57BL/6N mice, and vision scientists know to breed their knockout mice off of this background to establish precise ocular phenotyping of the genetic models that interest them. However, since the IMPC is the largest and most comprehensive source of single-gene knockout mice in the world, the vision science community will be tied to the C57BL6/N background, and the *rd8* mutation indefinitely, at least until each knockout is crossed onto an *rd8*-free background by independent investigators. Therefore, the background abnormalities associated with the C57BL/6N strain, and those associated with the *rd8* mutation, will be relevant to vision scientists for the foreseeable future.

Our aim was to quantify the frequency and severity of the different background ocular lesions in wild-type C57BL/6N mice, with specific attention given to variability seen in mice derived from various commercially available colonies. We provide vision scientists with a reference for future studies using the most widely produced and studied strain of mice. Such a large-scale examination of wild-type mouse eyes on the C57BL/6N background will prove to be highly useful as a foundation from which future genetic studies can be compared in knockout animals, especially those animals sourced from the IMPC.

Methods

Animals

C57BL/6N mice were obtained from various commercial sources with longstanding established colonies, including the Jackson Laboratory (Bar Harbor, ME, USA), Charles River Laboratories (L'Abresles, France), and Taconic Biosciences (Silkeborg, Denmark). These founders were used to establish local breeding colonies at each of the IMPC sites. Mutants and wild-type littermates were maintained in restricted, specific-pathogen–free vivaria on a 12:12-hour light-dark cycle. Animal care and use was conducted under guidelines provided by the eighth Revision of the Guide for the Care and Use of Laboratory Animals (Protocol No. 19075), and all procedures were performed according to the Association for Research in Vision and Ophthalmology Statement for the Use of Animals in Ophthalmic and Vision Research. Experiments carried out at the Institut Clinique de la Souris (animal facility agreement No. C67-218-40) were approved by the French Local Ethics Committee No. 17 and the French Ministry of Research (No. 2016040511578546) and performed in compliance with the European Community Regulation for Laboratory Animal Care and Use (Directive 2010/63/UE). For the purpose of this study, eye examination data were included only from wild-type C57BL/6N *rd8* control animals from the University of California at Davis (UCD) cohort (total 1877 mice; 941 males, 936 females). In addition, 896 mice were imaged in France across three colonies. Advanced ocular imaging using optical coherence tomography (OCT) was performed on 870 of these wild-type animals (452 males, 418 females) at the Institut Clinique de la Souris to determine central corneal thickness, anterior chamber depth, vitreous chamber depth, and retinal thickness.

For all mice, an initial, general systemic phenotyping schedule was initiated at 4 weeks of age. A more in-depth systemic phenotyping schedule, including ocular examination, was performed on mice aged 15 through 16 weeks, after which mice were euthanatized and tissues and blood were collected for anatomic and clinical pathology.[7] Rigorous standardized operating protocols (SOPs) were harmonized across all IMPC laboratories to ensure reproducible testing and data collection.[8] Phenotypic assessment and interpretation at all sites were made by personnel with specialized expertise in a variety of specific fields (e.g., pathology, ophthalmology, cardiology). Genotyping was performed for the *rd8* mutation at various times at each site by using the primers and methods described in the study of Mattapallil et al.[4] In every case, mice were found to be homozygous for the *rd8* mutation, which informed the decision not to perform genotyping for this allele as a matter of routine, as the commercial mouse providers maintained their breeding schemes.

Ophthalmic Phenotyping

Ophthalmic phenotyping followed an SOP developed for complete ophthalmic examinations of both eyes of each individual mouse at 15 to 16 weeks of age. The eye exams were performed on mixed, sex-balanced cohorts of knockouts and wild-type animals, which consisted of seven male and seven female homozygous knockout mice and two male and two female wild-type mice as controls. Examiners were masked to the genetic background of the mouse during examination. At the University of California-Davis, examinations were performed by veterinarians with advanced training in ophthalmology (BAM, AC, SGE, BCL, LS) with specific familiarity and knowledge of anticipated background lesions. New phenotypes outside of the C57BL/6N genetic background and mice with ocular abnormalities acquired secondarily to trauma and/or infection (e.g., corneal scars, periocular fur or eyelash loss, traumatic cataract) were excluded from the analysis presented here. All ocular findings were noted for every animal regardless of genotype, and all findings outside of an anticipated C57BL/6N background lesion were subsequently reviewed by board-certified veterinary ophthalmologists (CJM, SMT). The mice were gently restrained and neuro-ophthalmic (i.e., pupillary light reflexes), adnexal (i.e., the eyelids, third eyelid, conjunctiva), and anterior segment structures (i.e., cornea, iris, anterior sclera, and anterior chamber) were examined by slit lamp biomicroscopy at ×16 magnification by using broad-beam illumination at the highest intensity setting (Kowa SL-15; Kowa, Tokyo, Japan). Intraocular pressure (IOP) was measured by rebound tonometry (Tonolab; Icare Finland Oy, Vantaa, Finland). Following broad-beam anterior segment examination, the irides of all mice were pharmacologically dilated with either atropine 1% (Virbac, Carros, France) or a solution of 1:7 10% phenylephrine HCl (Akorn, Inc., Lake Forest, IL, USA) to 1% tropicamide (Bausch & Lomb, Inc., Tampa, FL, USA). The cornea, anterior chamber, lens, and vitreous chamber were then examined by slit lamp biomicroscopy at ×16 magnification by using a 0.1-mm slit beam at the highest intensity setting. Finally, fundus examination was performed via indirect ophthalmoscopy by using a portable indirect headset (Keeler AllPupil II LED Vantage Plus Wireless Headset; Keeler Instruments, Inc.,

Investigative Ophthalmology & Visual Science

Broomall, PA, USA) and a 60-diopter double aspheric handheld lens (Volk Optical, Inc., Mentor, OH, USA).

Ocular Imaging

A cocktail of either ketamine/midazolam (50–75/1–2 mg/kg), ketamine/xylazine (100/10 mg/kg), or ketamine/medetomidine (100/0.3 mg/kg) was administered intraperitoneally to induce anesthesia in all mice undergoing ocular imaging. A single drop of both tropicamide 1% and phenylephrine 2.5% (or atropine 1%) was used for dilation, and the ocular surface was lubricated with methylcellulose-containing artificial tears. Anterior segment images were obtained with a BQ900 slit lamp (Haag-Streit, Köniz, Switzerland), while fundus photographs were acquired with either Micron III (Phoenix Research Laboratories, Pleasanton, CA, USA) or topical endoscopic fundal imaging (TEFI).[9] OCT imaging was performed with an Envisu R2200 SD-OCT (spectral-domain OCT; Bioptigen-Leica, Wetzlar, Germany), after dilatation with a single drop of atropine 1% (Virbac, Carros, France). Thickness measurements of the retina (from the nerve fiber layer to the outer boundary of the retinal pigment epithelium [RPE]), its layers, and the vitreous chamber were performed at a distance of 0.5 mm from the optic nerve by using calipers in the InVivoVue 2.4 software (Bioptigen-Leica). Corneal thickness and cornea-lens distance (called hereafter anterior chamber depth) were measured in a similar way, along the eye axis. The presence of *rd8* lesions was determined on the OCT en face view obtained from the volume intensity projection of the outer retina. The severity of retinal dysplasia was qualitatively graded as mild (few pinpoint lesions), moderate (denser/larger lesions), or severe (most of the ventral quadrant or greater being affected with lesions).

Histology

For selected mice, eyes were either removed from the head or were fixed in situ in preparation for histology. Tissues were immersion fixed in 10% neutral-buffered formalin. If fixed in situ, the formalin-fixed heads were decalcified in 15% formic acid for at least 24 hours, until sufficient decalcification was achieved. Parasagittal sections of eyes or coronal sections through the head including eyes were processed routinely for histopathology, embedded in paraffin, sectioned 4- to 5-µm thick, and stained with hematoxylin-eosin. The histopathology was evaluated by a board-certified veterinary anatomic pathologist (DMI).

Statistics

For comparisons of groups of mice regarding IOP, or presence of retinal dysplasia, a 2-tailed Student's *t*-test was performed. A P value < 0.05 was considered statistically significant. The datasets generated and/or analyzed during the current study from UC Davis and France are available as Supplementary Material.

Results

Cornea

Corneal deposits were detected in 2.6% of wild-type C57BL/6N mice during slit lamp biomicroscopy. The deposits ranged in size from pinpoint to occupying up to 60% of the corneal surface (Fig. 1). The deposits were often well demarcated, horizontally ovoid, and formed by multifocal punctate to coalescing stromal crystalline white opacities. When examined by OCT the deposits appeared as a hyperreflective band in the corneal mid-stroma (Fig. 1E). No obvious histopathologic abnormalities were noted that would correlate with the corneal opacities, and no evidence of corneal mineralization was observed; however, possible corneal lipidosis was detected from larger, more rounded stromal clefts than what are normally described in mice.

Lens

Another commonly found lesion was a variable degree of anterior lens capsule translucency (Figs. 2A–C). The anterior lens capsule is normally more lucent than the cornea as viewed by slit-beam biomicroscopy (Fig. 2A). Decreased translucency of the anterior lens capsule ranged from equal optical density of the slit beam on the anterior lens capsule and corneal surface (Fig. 2B) to a markedly denser anterior lens capsule slit beam (Fig. 2C). We found that 33% of mice examined were normal (anterior lens capsule more lucent than cornea), and 67% had decreased anterior lens capsule translucency. Another background lesion found in the lens of C57BL/6N mice consisted of punctate nuclear cataracts (Figs. 2D, 2E), which were the most commonly seen background lesion with 98% of mice being affected. Histopathologically, the altered lens translucency was apparent as pale and flocculent anterior subcapsular lens fibers. Nuclear cataracts were described as disorganized, granular, and whorled nuclear lens fibers.

Vitreous

Vitreous opacities of two kinds are relatively common in C57BL/6N mice. Crystalline-like opacities within the anterior vitreous, sometimes in very close approximation to the posterior lens capsule (Fig. 3), were identified in 61% of eyes. Histologic sampling of these opacities was unable to be obtained. Vitreous pigmentation (Fig. 4) was detected commonly and was noted in two different forms. Axial pigment was noted infrequently (6%), either suspended within the vitreous or in association with the optic nerve or posterior lens capsule, findings characteristic of hyaloid vasculature remnants and/or persistent hyperplastic primary vitreous (Figs. 4A–C). These clinical findings were confirmed histologically. However, vitreous pigment most commonly appeared as small flecks located sporadically throughout the posterior vitreous near the retinal interface (Fig. 4D). These clinical findings were confirmed histologically (e.g., pigment flecks shown in Fig. 4D along with a persistent hyaloid vessel); however, the total number of animals possessing this distinct type of vitreal pigmentation was not documented.

Retina

C57BL/6N mice are nearly universally homozygous for the *rd8* mutation in the *Crb1* gene, which causes a variable amount of retinal dysplasia. These mice develop small multifocal to coalescing yellow flecks of varying degrees (e.g., mild [Figs. 5A, 5A'], moderate [Figs. 5B, 5B'], or severe [Figs. 5C, 5C']) that are predominantly located in the inferior nasal fundus. Histologically, folds and rosettes were present, primarily affecting the photoreceptor layer (Fig. 5D), which are not seen in areas lacking dysplastic flecks (Fig. 5D'). Systematic analysis of the en face view of OCT data from 1792 eyes of C57BL/6N mice (summed from Taconic, Charles River-A, and Charles River-B colonies in France) revealed that 75.9% had no *rd8* lesions in the area centered on the optic nerve. Among the 24.1% of animals that did have an *rd8* phenotype on photos, these were divided into 21.0% mild, 1.3% moderate, and 1.7% severe *rd8* phenotype as shown in Figure 5.

Investigative Ophthalmology & Visual Science

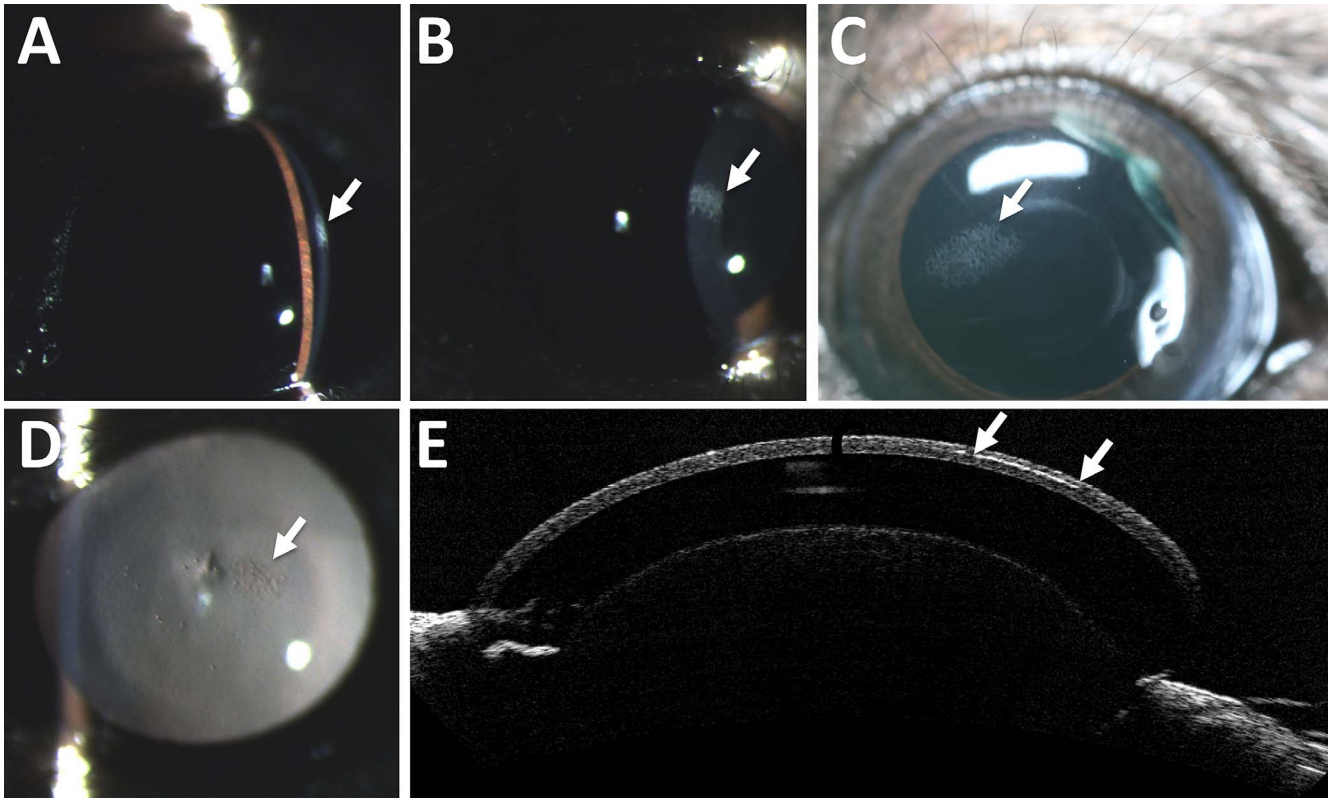

Figure 1. Corneal abnormalities commonly seen in C57BL/6N mice. Corneal deposits seen on slit lamp exam ranged from punctate in size to affecting nearly 60% of the corneal surface. Moderately sized corneal opacities are shown here with a 0.1-mm slit beam (**A**), a 0.8-mm slit beam (**B**), by direct inspection (**C**), and on retroillumination (**D**). *Arrows* point to the area of interest in (**A**–**D**). When examined by optical coherence tomography (**E**), the deposits appear to form a curvilinear hyperreflective opacity in the corneal stroma, seen between the two *arrows*.

Interestingly, we observed a higher percentage of *rd8* lesions in male animals (29.6%) than in female animals (17.8%) when combining all animals from all three colonies (Taconic, Charles River-A, and Charles River-B) in France. This pattern of male predominance was consistently observed across all three C57BL/6N colonies in France, though to varying degrees (Table). Interestingly, there was a significant difference between mice obtained from two different providers: only 15.0% of eyes of those obtained from Charles River were affected (157 of 1046), compared to 26.7% of eyes of those obtained from Taconic (274 of 746). The cause and mechanism of the sexual dimorphism seen in these animals are not known.

In contrast to the more limited view obtained during fundus photography and/or OCT, indirect ophthalmoscopy enables the examiner to evaluate the entire retinal landscape. When indirect ophthalmoscopy was used on 1877 mice (3754 eyes) from a fourth independent colony of C57BL/6N mice at UC Davis to determine the presence of *rd8* retinal lesions, we found that 1850 eyes (49%) had some evidence of retinal dysplasia. Since some animals only had one affected eye at the time of ocular examination, the rate of affected animals was higher than the rate of affected eyes: overall, 1087 of 1877 animals (58%) had at least one eye with evidence of retinal dysplasia by indirect ophthalmoscopy. The degree of retinal dysplasia seen on indirect ophthalmoscopy was not graded in this fourth cohort. The increased rate of retinal dysplasia detected by indirect ophthalmoscopy, compared to the rate seen on fundus photos/OCT analysis, may be due to the more limited field of view obtained during imaging, which does not capture the peripheral retina. The pattern of increased penetrance of the retinal phenotype in males compared to females was confirmed in the UC Davis colony (Table). The prevalence of dysplasia in the UC Davis colony was 1097 of 1882 (58%) in male eyes, while 822 of 1872 (44%) female eyes were affected. In male mice, 597 of 941 animals (63%) had at least one affected eye, compared to 490 of 936 (52%) in female animals.

Several infrequent ocular anomalies were also observed. Notably, microphthalmia and dyscoria/corectopia were described in approximately 1% to 2% of mice. Other rare anomalies included severely atrophic retina. These rare anomalies described here are likely sporadic and not inherent background lesions of this mouse strain.

Optical Coherence Tomography Measurements

SD-OCT measurements are represented in Figure 6, including retinal thickness and manual segmentation of various retinal layers, vitreous thickness, anterior chamber depth, and corneal thickness. The average measurements of these ocular compartments and tissues were based on 1466–1736 eyes, and the results of these measurements are summarized in Figure 6. Central corneal thickness was 88 ± 11 μm, and anterior chamber depth was 411 ± 17 μm, vitreous depth was 530 ± 18 μm, and retinal thickness was 223 ± 5 μm. OCT is capable of producing nearly histologic-quality thickness measurements of the retina (223 ± 5 μm) and its various constitutive layers: inner plexiform layer (IPL; 61 ± 4 μm), inner nuclear layer (INL; 29 ± 3 μm), outer nuclear layer (ONL; 58 ± 3 μm), and photoreceptor inner/outer segments (40.0 ± 3 μm), all measured at 0.5 mm from the optic nerve head.

Investigative Ophthalmology & Visual Science

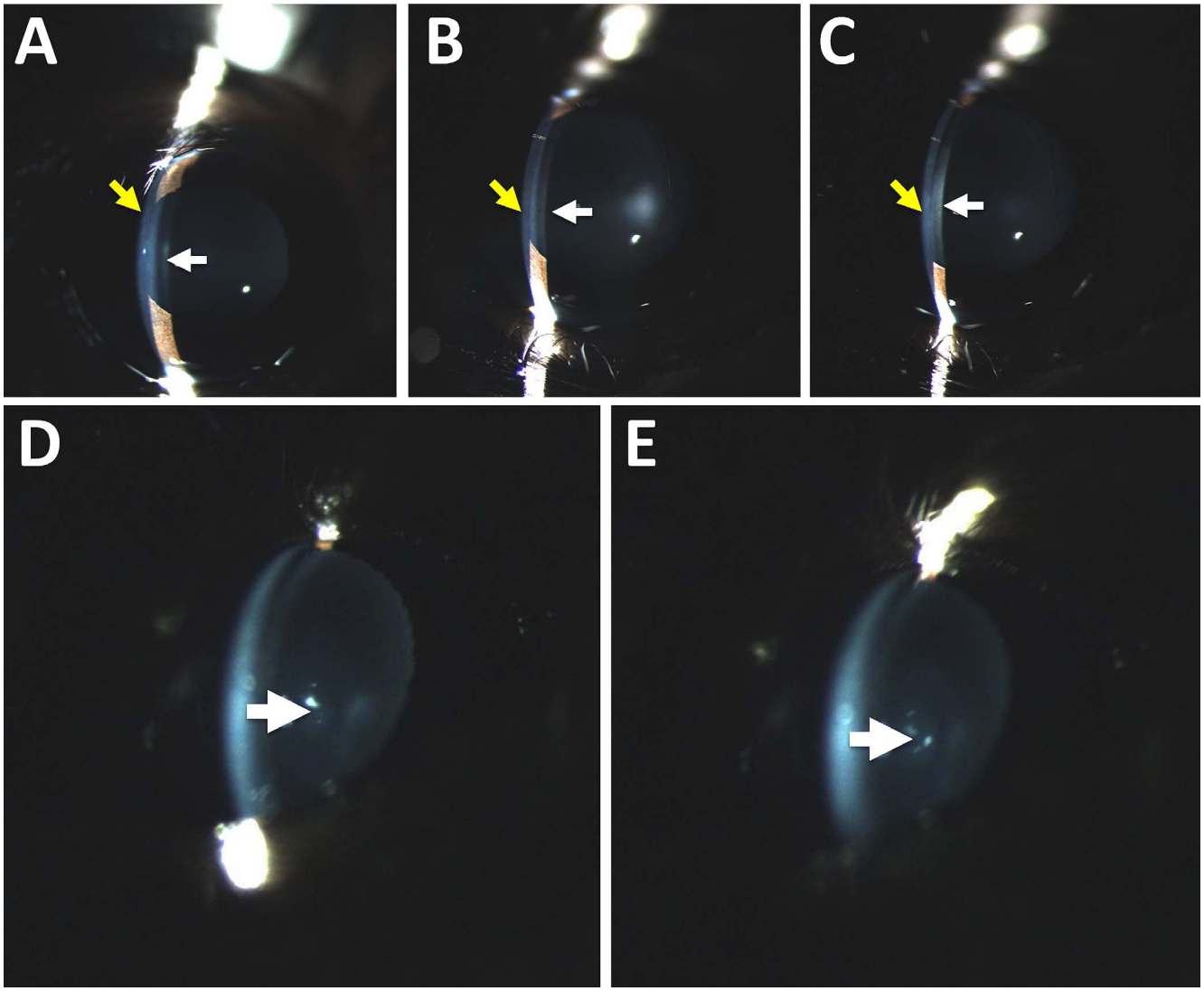

Figure 2. Lenticular abnormalities commonly seen in C57BL/6N mice. Increased optical density of the anterior lens capsule is common in adult mice of this strain. The normal translucence of the cornea and anterior lens capsule is shown in (**A**), where the anterior lens capsule (*white arrow*) is more lucent (less optically dense) than the cornea (*yellow arrow*), based on slit beam biomicroscopy. Abnormally increased anterior lens capsule translucencies are shown as being equally optically dense to the corneal slit beam (**B**) or more optically dense than the corneal slit beam (**C**). Furthermore, punctate nuclear opacities (**D**, **E**) are seen in nearly every mouse of the C57BL/6N strain (*white arrows* point to three or four small nuclear cataracts).

Intraocular Pressure

IOP in C57BL/6N mice was measured and found to be 10.9 mm Hg ± 1.9 SD with no significant differences between males and females or between the right and left eyes (Fig. 7).

Discussion

We characterized the background ocular lesions present in C57BL/6N mice along with their relative frequency by examining 5546 wild-type eyes from 2773 mice (roughly equal numbers of females and males) at 15 to 16 weeks of age. The value of the findings presented here will only increase as the IMPC continues to grow as a major resource for knockout mice that have already been created and phenotyped. With the increased utilization of C57BL/6N genetic knockouts from IMPC centers for more detailed ophthalmic analysis and characterization, the background abnormalities common in the C57BL/6N strain must be well understood, as the presence of background lesions can confound phenotypic screening of genetic knockouts. Results from this large population screen provide a valuable reference standard for vision scientists using C57BL/6N mice.

Corneal opacities were noted infrequently as a background lesion in C57BL/6N mice (Fig. 1). For most strains of mice, reports of congenital corneal defects typically involve a relationship with the lens (e.g., delayed or abnormal keratolenticular cleavage/separation from the lens vesicle) or in association with more global ocular abnormalities such as microphthalmia.[10] However, we identified discrete, anterior stromal deposits that ranged in size from pinpoint to affecting up to 60% of the corneal area. The C57BL strain of mice has been reported to have a background corneal lesion that consists of a stromal defect with disorganized overlying epithelium.[10] The corneal lesions documented here appear to be an anterior to mid-stromal deposit without epithelial

Investigative Ophthalmology & Visual Science

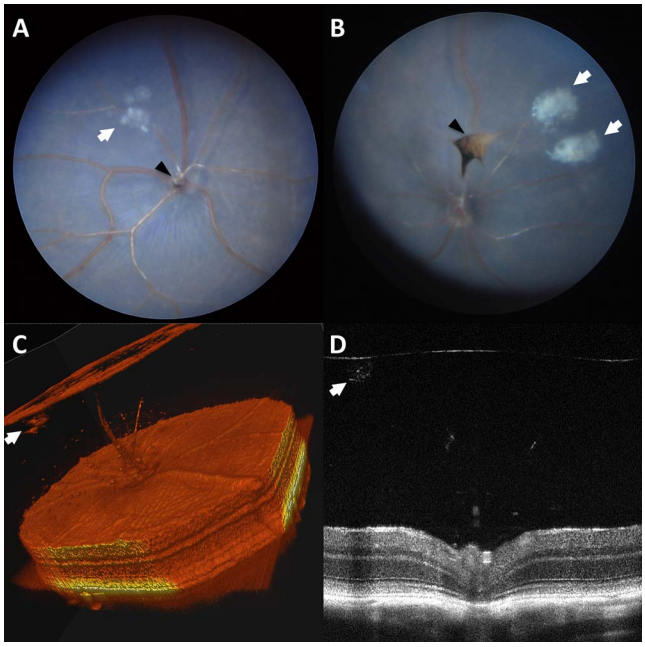

Figure 3. Vitreous crystalline deposits seen in C57BL/6N mice. Vitreous crystalline opacities of various sizes appearing in a celestial pattern (*white arrows*) in fundus photographs (**A**, **B**). 3D-rendered OCT (**C**) and standard cross-sectional OCT imaging (**D**). Incidental vitreous pigment (*black arrowheads*) can be seen (**A**, **B**).

disorganization as based on OCT. The limited histologic findings were suggestive of lipid deposits.

Lens abnormalities were extremely common in C57BL/6N mice. More than half of the eyes examined (67%) had a decreased translucency of the anterior lens capsule relative to the cornea (Figs. 2A–C). These altered translucencies are not true cataracts, as light is able to pass through them; however, the altered translucencies when severe would subtly impede light, and with time could progress toward capsular cataract formation. Histologically, severe altered translucencies were described as having subtly pale and flocculent anterior capsular cataracts, but no histopathologic findings could be detected in mild or moderate forms. It has been reported that decreased anterior lens translucency and even cataract formation can occur after anesthesia in mice, which has been demonstrated to be a result of tear film evaporation and a subsequent rise in aqueous humor osmolarity.[11] Our assessment is that lens changes were primary in nature rather than a consequence to drugs and/or dessication. All mice were examined without sedation or anesthesia and mice retained the ability to blink throughout examinations, and it is unlikely that topical administration of a mydriatic agent would result in an increased aqueous osmolarity significant enough to cause lens opacification. Furthermore, decreased lens translucency was detected before pharmacologic pupil dilation. Lens opacities are an extremely common background lesion in mice that have rapidly increased in reported frequency in the past 30 years owing to extensive manipulation of the mouse genome.[12] The lens nucleus of mice is less easily distinguished than that of humans in nonpathologic conditions. By far the most common lens abnormality in C57BL/6N mice is nuclear cataracts, which were found in nearly every mouse examined (98%; Figs. 2D, 2E).

The vitreous was affected with a high frequency of abnormalities in the form of both crystalline deposits and pigment. Crystalline deposits were common (61%) in the vitreous chamber of C57BL/6N mice. Several mutations are known to be associated with lenticular crystalline opacities within the vitreous chamber due to posterior lens capsule rupture,[13–16] which often results in rapid increase in cataract density but not marked intraocular inflammation like that observed in humans.[14] Although the crystalline opacities described here typically occurred in the anterior vitreous, often in close proximity to the posterior lens (Fig. 3), they occurred without evidence of any posterior lens capsule rupture. These structures were not detected via light microscopy. Pigmentation in the vitreous chamber was present in two forms: small scattered pigment and pigment associated with incomplete regression of the hyaloid vasculature or persistent hyperplastic primary vitreous. The most common form of pigment detected was found scattered throughout the vitreous chamber in small or large aggregates (Fig. 4). Pigmentation overlying the optic nerve, often attached via a stalk, or adhered to the posterior pole of the lens (sometimes with associated posterior capsular cataract), likely represents a remnant of the hyaloid vasculature or persistent primary hyperplastic vitreous (Fig. 4C).

IOP was remarkably uniform in C57BL/6N mice. Most studies of IOP require sedation/anesthesia, but with proper restraint and use of a rebound tonometer we were able to assess IOP reliably. The rebound tonometry measurements were found to be consistent with previous reports of IOP in wild-type mice, using similar methods.[17]

The OCT measurements of the thicknesses of ocular tissues and spaces represent a significant contribution to the vision science community, especially regarding C57BL/6N mice, and probably to the murine eye in general. Other studies have reported retinal thickness measurements on various strains of mice,[18–25] but differences in OCT devices, authors' preferenc-

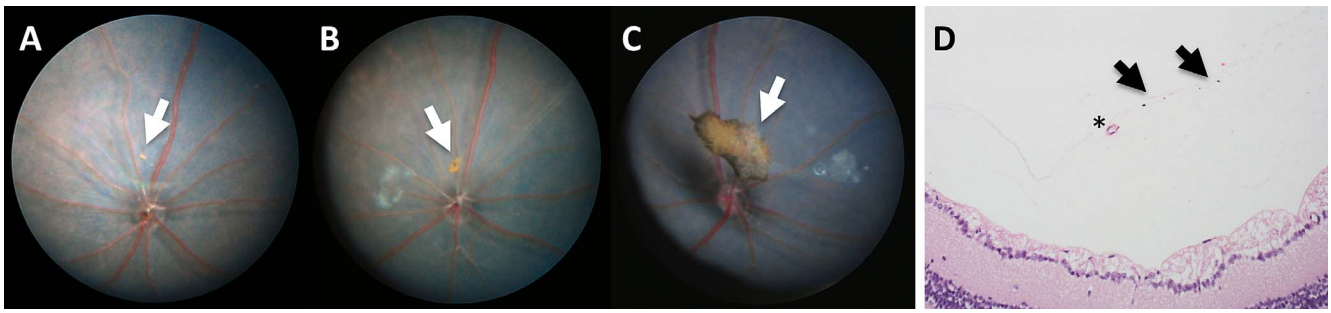

Figure 4. Vitreous pigment is commonly seen in C57BL/6N mice. Vitreous pigmentation located axially and often in association with the pole of the posterior lens capsule or optic nerve head (**A–C**; *white arrows*) is characteristic of persistent hyaloid vasculature or persistent hyperplastic primary vitreous. Also commonly found are punctate dispersed pigment flecks located throughout the vitreous chamber (**D**; *black arrows*). Additionally, (**D**) shows an example of an isolated blood vessel, representative of persistent hyaloid vasculature (*asterisk*).

Investigative Ophthalmology & Visual Science

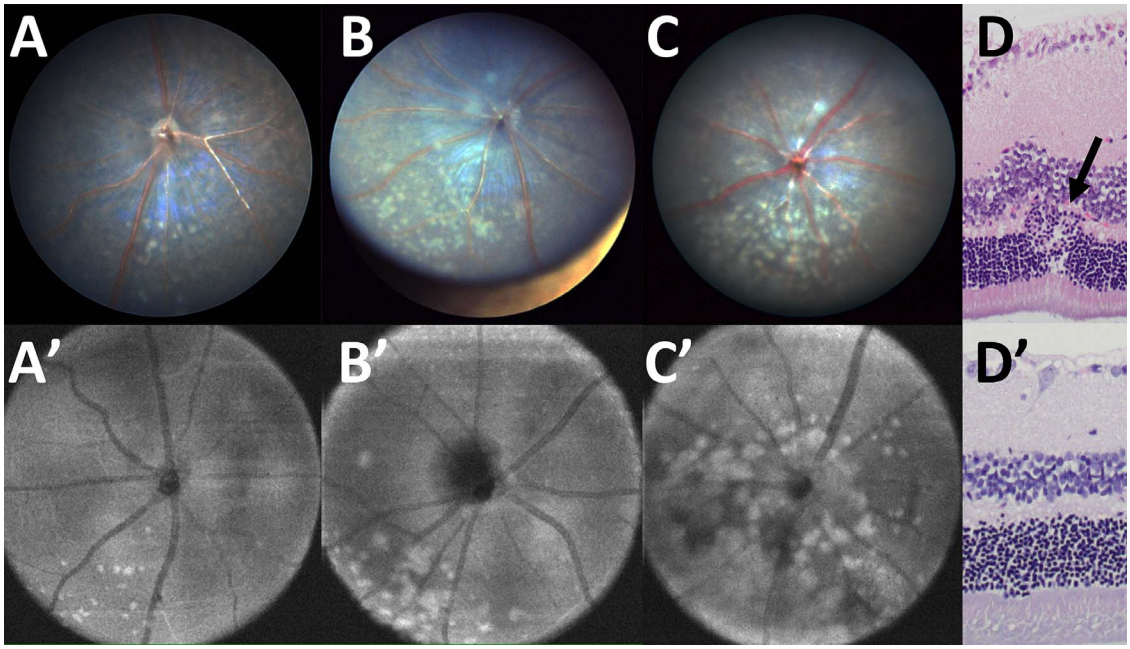

Figure 5. Different grades of retinal dysplasia found in C57BL/6N mice with the *rd8* mutation. The degree of retinal dysplasia can be graded from mild (**A**, **A'**), moderate (**B**, **B'**), to severe (**C**, **C'**) dysplasia. Histologically, retinal folds and/or rosettes are noted in areas of lesions (**D**), but are not seen in unaffected areas (**D'**). Images in (**A**–**C**) are TEFI images, while (**A'**–**C'**) are en face OCT images.

es regarding segmentation and groupings of the various retinal layers, and the way the authors chose to present the quantitative OCT data are all variables that make direct comparisons between studies difficult. One study using mice designated simply as C57BL/6 reports retinal measurements using the same instrument and in a similar fashion as those presented here, and is perhaps the most appropriate reference for comparison.[26] They report a total retinal thickness (retina 204.4 μm + RPE 18.2 μm) of 222.6 μm (compared to our 223.1 μm), IPL thickness of 59.6 μm (compared to our 60.8 μm), INL thickness of 27.8 μm (compared to our 28.6 μm), and ONL thickness of 62.8 μm (compared to our 58.2 μm). While the measurements between these two studies are very similar, differences may be due to their study having been done using just 30 male mice purchased from the Jackson Laboratory (Bar Harbor, ME, USA), which may have been 6J and may not have had retinal abnormalities.

C57BL/6N mice are homozygous for the *rd8* mutation in *Crb1* (Crumbs homolog 1) gene. The *rd8* mutation is a single-nucleotide deletion causing a frame shift, leading to an early stop codon and nonfunctional gene product.[27] This gene is a cell surface membrane-bound protein required for the correct determination of cell polarity in several tissues, most notably in photoreceptors of the mammalian retina. Crb1 localizes primarily to the subapical region (SAR) of Müller glial cells and, to a lesser extent, to the SAR of the photoreceptors. It is known to interact directly with the protein associated with Lin seven 1 (*Pals1*), and through it, with the Pals1-associated tight junction protein (*Patj*), and the multi-PDZ domain protein 1 (*Mupp1*), to form tight junctions at the SAR and to maintain the integrity of the external limiting membrane.[28,29] Retinal dysplasia of C57BL/6N mice is attributed to the *rd8* mutation in *Crb1*, leading to a variable degree of rosette formation due to photoreceptor polarity defects. The dysplastic changes are consistently most prominent in the inferior retina.

Despite the presence of retinal dysplasia, even with marked histologic changes, affected *rd8* mice have relatively normal full-field electroretinograms.[18] It is reported that the severity of the phenotype in *rd8* mice varies from retina to retina, and the degeneration of B6N *rd8* mice is less severe than in the $Crb1^{-/-}$ retinas.[30] However, humans with *CRB1* mutations develop autosomal recessive retinitis pigmentosa, or are born blind owing to Leber's congenital amaurosis (LCA8), both severe photoreceptor diseases. *CRB1* mutations typically

Table. Sexual Dimorphism in Penetrance of *rd8* Phenotype in C57BL/6N Mice

	Taconic	Charles River-A	Charles River-B	UC Davis
Males rd8 affected	183	32	65	1028
Males total	372	396	178	1882
Males rd8 affected, %	49	8	37	55
Females rd8 affected	91	15	45	822
Females total	374	287	185	1872
Females rd8 affected, %	24	5	24	44
P value	0.00000000000046	0.0995	0.0114	0.00000000004675

Penetrance of the *rd8* phenotype was increased in males in all four colonies used in this study, though the Charles River-A colony did not meet statistical significance, perhaps owing to the relatively low overall rate of affected animals. The number listed in each group is the number of eyes. Comparisons between male and female eyes within each colony were made with a Student's *t*-test. *P* value < 0.05 was considered statistically significant. Taconic and Charles River Laboratories–based colonies (A and B) are in France. The UC Davis colony is in the United States (California).

Investigative Ophthalmology & Visual Science

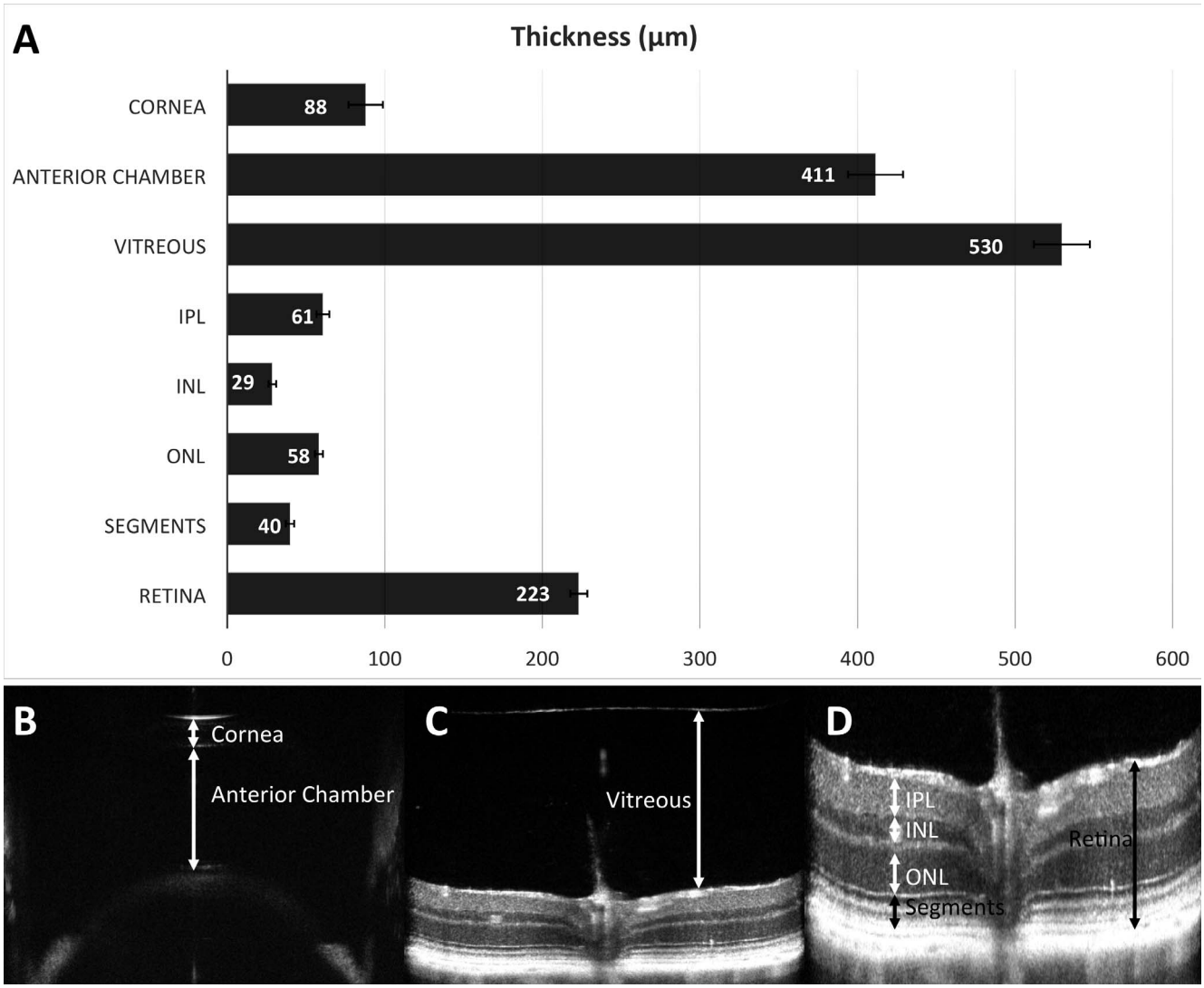

Figure 6. Average measurements of the thickness of ocular tissues and compartments from a population of C57BL/6N mice, using OCT. Anterior segment OCT determined the central corneal thickness (88 ± 11 μm, $n = 1466$) and anterior chamber depth (411 ± 17 μm, $n = 1506$). The vitreous depth was assessed (530 ± 18 μm, $n = 1698$). Overall retinal thickness was measured (223 ± 5 μm, $n = 1736$). Segmentation of retinal layers, at the level of the optic nerve, quantified thicknesses of the inner plexiform layer (61 ± 4 μm, $n = 1736$), inner nuclear layer (29 ± 3 μm, $n = 1736$), outer nuclear layer (58 ± 3 μm, $n = 1736$), and photoreceptor inner/outer segments (40.0 ± 3 μm, $n = 1736$). *Error bars* (**A**) represent standard deviation. Examples of measurements of corneal thickness and anterior chamber depth (**B**) are shown. (**C**) An example of manual measurement of central vitreous depth is shown. (**D**) An example of measurement of retinal thickness and manual segmentation of retinal layers. *N* represents the number of eyes. Retina, total retinal thickness; segments, photoreceptor inner and outer segments.

exhibit a more severe retinal phenotype than *CRB2* in humans, though a minority of patients with CRB2-related syndrome have congenital retinal and/or optic nerve disease.[31] In mice, the Crb1 deficiency is less severe than in humans, because photoreceptor expression of Crb2 compensates for the absence of Crb1 in this species. Consistent with this explanation, mice lacking both Crb1 and Crb2 have severe photoreceptor degeneration more similar to the human CRB1 phenotype of LCA.[32] CRB2 is not expressed in human photoreceptors, but rather only in Müller glial cells.[33] For this reason, humans with *CRB1* mutations typically develop more severe degeneration than that seen in mice.[34,35]

We have also observed that while all C57BL/6N mice are homozygous for the *rd8* mutation, the phenotype is variably penetrant at the time of ocular examination (4 months postnatally). Furthermore, the *rd8* background does not always worsen the retinal degeneration phenotype of all knockout mouse models of retinal disease.[36] The variable penetrance of the retinal dysplasia phenotype is also correlated with the location from where the mice were obtained. For example, the mice derived from Taconic had a more severe and more frequent dysplasia phenotype than animals from Charles River Laboratories. It has been shown previously that the *rd8* phenotype is modified by genetic and epigenetic factors.[37] We attribute the variability in the retinal phenotype to genetic drift and mutation of unknown presumed modifying genes and epigenetic factors, which either amplify or dampen the photoreceptor disease.

Retinal dysplasia in the C57BL/6N mice is rightfully attributed to the *rd8* mutation, but the other ocular phenotypes described here may also be related to Crb1, or may be due to other genetic factors on this inbred strain. Since advanced anterior segment phenotyping occurred in the UC Davis cohort, and detailed fundus grading occurred on mice in

Investigative Ophthalmology & Visual Science

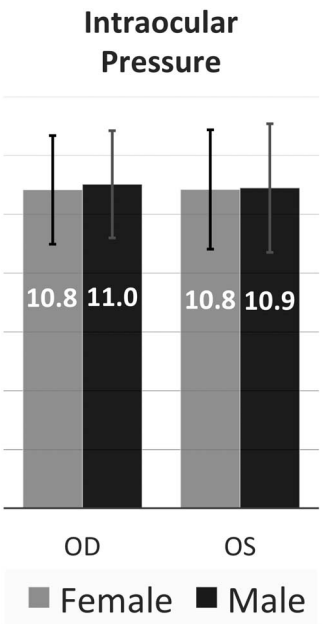

Figure 7. Intraocular pressure measurements. The mean intraocular pressure across all measured eyes was 10.9 mm Hg ± 1.9 SD (n = 1082). Male eye IOP (mean, 10.9; n = 436) and female eye IOP (mean, 10.8; n = 646) were indistinguishable. The mean IOP of left and right eyes of each sex is shown on the graph. *Error bars* represent standard deviation. *N* represents the number of eyes.

France, it is not possible to draw statistically meaningful conclusions regarding possible correlations between the frequency and severity of anterior segment abnormalities and posterior segment abnormalities in the same eyes. However, OCT of mice with severe retinal dysplasia did not seem to correlate with the presence of vitreous opacities (data not shown). Determining if the *rd8* mutation is responsible for not only the retinal dysplasia in C57BL6N mice, but also the other common ocular abnormalities described in this report, is a matter of future investigation. Future studies could also evaluate the heterogeneity and frequency of background eye lesions in other strains, in order to determine which strains have the least variation and are therefore more ideal choices for modeling the genetics of ocular disease.

The value of this report lies in the systematic documentation of the spectrum and frequency of ocular findings. We acknowledge that both a strength and limitation of the study was the specific age range (15–16 weeks), and it is possible that progression of lesions identified and appearance of new lesions could occur with advancing age. As OCT becomes more and more prevalent, there is a need for established normative data of ocular structures in the C57BL/6N strain of mice. We hope that the large numbers of animals involved in this study, the systematic nature in which the examinations were performed, the proficiency of the examiners, and the precision of the advanced imaging measurements will combine to make these data an important benchmark for our colleagues in the vision science community.

Acknowledgments

The authors thank Steven Hollingsworth for his support and Monica Motta for excellent technical assistance; Mike Schuchbauer, Heather Tolentino, Todd Tolentino, and Amanda Trainor (University of California-Davis), Chaouki Bam'Hamed, Raphaël Bour, Alain Guimond, and Aline Lux (ICS) for assistance with eye examinations; and Esi Djan, Alison Huynh, and Milton Pham for assistance in necropsy and slide preparation.

Supported by the National Institutes of Health/National Eye Institute (NIH NEI) K08EY027463 Mentored Career Development Award (AM), the NIH NEI K08EY021142 Mentored Career Development Award (SMT), the Research to Prevent Blindness (RPB) Career Development Award, International Retina Research Foundation research grant (AM), NIH OD UM1OD023221 (KCKL), the National Centre for Scientific Research (CNRS); the French National Institute of Health and Medical Research (INSERM); the University of Strasbourg (UDS); the Centre Européen de Recherche en Biologie et en Médecine; the French state funds through the "Agence Nationale de la Recherche" under the framework program "Investissements d'Avenir" labeled ANR-10-IDEX-0002-02, ANR-10-INBS-07 PHENOMIN (YH).

Disclosure: **B.A. Moore**, None; **M.J. Roux**, None; **L. Sebbag**, None; **A. Cooper**, None; **S.G. Edwards**, None; **B.C. Leonard**, None; **D.M. Imai**, None; **S. Griffey**, None; **L. Bower**, None; **D. Clary**, None; **K.C.K. Lloyd**, None; **Y. Hérault**, None; **S.M. Thomasy**, None; **C.J. Murphy**, None; **A. Moshiri**, None

References

1. Brown SD, Moore MW. Towards an encyclopaedia of mammalian gene function: the International Mouse Phenotyping Consortium. *Dis Model Mech*. 2012;5:289–292.
2. Brown SD, Moore MW. The International Mouse Phenotyping Consortium: past and future perspectives on mouse phenotyping. *Mamm Genome*. 2012;23:632–640.
3. Smith RS, Sundberg JP. Strain background disease characteristics. In: John SWM, Nishina PM, Smith RS, Sundberg J, eds. *Systemic Evaluation of the Mouse Eye: Anatomy, Physiology, and Biomethods*. Boca Raton, FL: CRC Press; 2002:67–75.
4. Mattapallil MJ, Wawrousek EF, Chan CC, et al. The Rd8 mutation of the Crb1 gene is present in vendor lines of C57BL/6N mice and embryonic stem cells, and confounds ocular induced mutant phenotypes. *Invest Ophthalmol Vis Sci*. 2012;53:2921–2927.
5. den Hollander AI, Ghiani M, de Kok YJ, et al. Isolation of Crb1, a mouse homologue of Drosophila crumbs, and analysis of its expression pattern in eye and brain. *Mech Dev*. 2002;110:203–207.
6. van de Pavert SA, Kantardzhieva A, Malysheva A, et al. Crumbs homologue 1 is required for maintenance of photoreceptor cell polarization and adhesion during light exposure. *J Cell Sci*. 2004;117:4169–4177.
7. Kurbatova N, Mason JC, Morgan H, Meehan TF, Karp NA. PhenStat: a tool kit for standardized analysis of high throughput phenotypic data. *PLoS One*. 2015;10:e0131274.
8. Karp NA, Meehan TF, Morgan H, et al. Applying the ARRIVE guidelines to an in vivo database. *PLoS Biol*. 2015;13:e1002151.
9. Paques M, Guyomard JL, Simonutti M, et al. Panretinal, high-resolution color photography of the mouse fundus. *Invest Ophthalmol Vis Sci*. 2007;48:2769–2774.
10. Pierro LJ, Spiggle J. Congenital eye defects in the mouse I: corneal opacity in C57black mice. *J Exp Zool*. 1967;166:25–38.
11. Ridder W III, Nusinowitz S, Heckenlively RJ. Causes of cataract development in anesthetized mice. *Exp Eye Res*. 2002;75:365–370.
12. Smith RS, Sundberg JP, Linder CC. Mouse mutations as models for studying cataracts. *Pathobiology*. 1997;65:146–154.
13. Beasley AB. Inheritance and development of a lens abnormality in the mouse. *J Morphol*. 1963;112:1–11.
14. Fraser FC, Herer ML. The inheritance and expression of the 'lens rupture' gene in the house mouse. *J Hered*. 1950;41:3.

15. Fraser FC, Herer ML. Lens rupture, a new recessive gene in the house mouse. *J Hered*. 1948;39:149.
16. Runge PE, Hawes HL, Heckenlively JR, Langley SH, Roderick TH. Autosomal dominant mouse cataract (Lop-10): consistent differences of expression in heterozygotes. *Invest Ophthalmol Vis Sci*. 1992;33:3202–3208.
17. Kim CY, Kuehn MH, Anderson MG, Kwon YH. Intraocular pressure measurement in mice: a comparison between Goldmann and rebound tonometry. *Eye (Lond)*. 2007;21:1202–1209.
18. Aleman TS, Cideciyan AV, Aguirre GK, et al. Human CRB1-associated retinal degeneration: comparison with the rd8 Crb1-mutant mouse model. *Invest Ophthalmol Vis Sci*. 2011;52:6898–6910.
19. Antony BJ, Jeong W, Abràmoff MD, Vance J, Sohn EH, Garvin MK. Automated 3D segmentation of intraretinal surfaces in SD-OCT volumes in normal and diabetic mice. *Trans Vis Sci Tech*. 2014;3(5):8.
20. Bell BA, Kaul C, Bonilha VL, Rayborn ME, Shadrach K, Hollyfield JG. The BALB/c mouse: effect of standard vivarium lighting on retinal pathology during aging. *Exp Eye Res*. 2015;135:192–205.
21. Berger A, Cavallero S, Dominguez E, et al. Spectral-domain optical coherence tomography of the rodent eye: highlighting layers of the outer retina using signal averaging and comparison with histology. *PLoS One*. 2014;9:e96494.
22. Li Y, Fariss RN, Qian JW, Cohen ED, Qian H. Light-induced thickening of photoreceptor outer segment layer detected by ultra-high resolution OCT imaging. *Invest Ophthalmol Vis Sci*. 2016;57:OCT105–OCT111.
23. Pennesi ME, Michaels KV, Magee SS, et al. Long-term characterization of retinal degeneration in rd1 and rd10 mice using spectral domain optical coherence tomography. *Invest Ophthalmol Vis Sci*. 2012;53:4644–4656.
24. Puk O, de Angelis MH, Graw J. Longitudinal fundus and retinal studies with SD-OCT: a comparison of five mouse inbred strains. *Mamm Genome*. 2013;24:198–205.
25. Fischer MD, Huber G, Beck SC, et al. Noninvasive, in vivo assessment of mouse retinal structure using optical coherence tomography. *PLoS One*. 2009;4:e7507.
26. Ferguson LR, Dominguez JM II, Balaiya S, Grover S, Chalam KV. Retinal thickness normative data in wild-type mice using customized miniature SD-OCT. *PLoS One*. 2013;8:e67265.
27. Mehalow AK, Kameya S, Smith RS, et al. CRB1 is essential for external limiting membrane integrity and photoreceptor morphogenesis in the mammalian retina. *Hum Mol Genet*. 2003;12:2179–2189.
28. van Rossum AG, Aartsen WM, Meuleman J, et al. Pals1/Mpp5 is required for correct localization of Crb1 at the subapical region in polarized Muller glia cells. *Hum Mol Genet*. 2006;15:2659–2672.
29. Richard M, Roepman R, Aartsen WM, et al. Towards understanding CRUMBS function in retinal dystrophies. *Hum Mol Genet*. 2006;15:R235–R243.
30. Chu XK, Wang Y, Ardeljan D, Tuo J, Chan CC. Controversial view of a genetically altered mouse model of focal retinal degeneration. *Bioengineered*. 2013;4:130–135.
31. Lamont RE, Tan WH, Innes AM, et al. Expansion of phenotype and genotypic data in CRB2-related syndrome. *Eur J Hum Genet*. 2016;24:1436–1444.
32. Pellissier LP, Alves CH, Quinn PM, et al. Targeted ablation of CRB1 and CRB2 in retinal progenitor cells mimics Leber congenital amaurosis. *PLoS Genet*. 2013;9:e1003976.
33. Pellissier LP, Lundvig DM, Tanimoto N, et al. CRB2 acts as a modifying factor of CRB1-related retinal dystrophies in mice. *Hum Mol Genet*. 2014;23:3759–3771.
34. den Hollander AI, Heckenlively JR, van den Born LI, et al. Leber congenital amaurosis and retinitis pigmentosa with Coats-like exudative vasculopathy are associated with mutations in the crumbs homologue 1 (CRB1) gene. *Am J Hum Genet*. 2001;69:198–203.
35. Lotery AJ, Jacobson SG, Fishman GA, et al. Mutations in the CRB1 gene cause Leber congenital amaurosis. *Arch Ophthalmol*. 2001;119:415–420.
36. Sahu B, Chavali VR, Alapati A, et al. Presence of rd8 mutation does not alter the ocular phenotype of late-onset retinal degeneration mouse model. *Mol Vis*. 2015;21:273–284.
37. Luhmann UF, Carvalho LS, Holthaus SM, et al. The severity of retinal pathology in homozygous Crb1rd8/rd8 mice is dependent on additional genetic factors. *Hum Mol Genet*. 2015;24:128–141.

Investigative Ophthalmology & Visual Science